Article

Not peer-reviewed version

Changjiang River (China) Suspended Sediment Concentration Estimation with Sentinel-2

Michael Nones * and Chao Guo

Posted Date: 15 May 2024

doi: 10.20944/preprints202405.1032.v1

Keywords: Changjiang River; suspended sediment concentration; Sentinel-2; reflectance bands

Article

Changjiang River (China) Suspended Sediment Concentration Estimation with Sentinel-2

Michael Nones [1,*] and Chao Guo [2]

[1] Institute of Geophysics Polish Academy of Sciences, Warsaw, Poland; mnones@igf.edu.pl
[2] Changjiang River Scientific Research Institute, Wuhan, China; guoc@mail.crsri.cn
* Correspondence: mnones@igf.edu.pl

Abstract: Spatiotemporal variations of sediments transported along rivers play a crucial role in a wide spectrum of uses, such as navigation, recreation, habitats or hydropower production. The advancement in technology has made it possible to use various indirect techniques to study and evaluate the transport of suspended sediment in fluvial environments. To investigate large-scale phenomena, remote sensing is becoming a largely utilized approach, as it allows to combine spatially-distributed and local information. Dam-induced sediment reduction occurs in large and small rivers worldwide, having profound implications on the fluvial systems. However, the systematic change of suspended sediment concentration (SSC) and its dynamic processes are not well known, and generally investigated only at the very local scale using field information. In this work, SSC maps were created by combining satellite images with local monitoring SSC data, using the Zhijiang -Chenglingji reach of the Changjiang River (China) as a case study, and analyzing how SSC dynamics changed over the period 2017-2022 in correspondence of extreme events. Multiple relationships between measured SSC and bands reflectance were tested, showing the potential of the best-performing one (R^2=0.43) in mapping SSC spatiotemporal variations over an extent of dozens of kilometres, eventually providing new insights into the SSC dynamics at hotspots of the river systems, such as confluence zones, barriers, and reservoirs.

Keywords: Changjiang River; suspended sediment concentration; Sentinel-2; reflectance bands

1. Introduction

Sediment plays a crucial role in shaping fluvial systems, influencing the quality of habitats, determining the morphology of rivers, and impacting various uses of watercourses such as energy production, navigation, and drinking water supply. Therefore, it is essential to comprehend both the morphological changes in the river planform and the sediment transport processes. Quantitative data about the transported sediment and channel variations are necessary for understanding river dynamics at various spatiotemporal scales, as well as for engineering and ecological studies related to rivers. For instance, this information can be used to plan river restoration measures or hydraulic infrastructures and to investigate changes in water quality driven by sediment variations.

For many years, measuring the amount of suspended sediment in rivers has been an important way to determine erosion and the river's ability to shape the landscape [1–3]. The suspended sediment concentration (SSC) also has a significant impact on river ecosystems. It controls the amount of sunlight that reaches the water, which in turn affects the growth of vegetation and algae [4]. Additionally, SSC affects the suitability of habitats, fish migration, and the way estuaries form and change. Suspended sediment also carries carbon, nutrients, and contaminants [5–8]. Tracking SSC levels can provide insights into the dynamics of pollutants such as microplastics [9,10], which are the focus of innovative policies such as the European Zero Pollution Action Plan.

The impact of natural variations and anthropogenic activities on SSC trends is rarely discussed, even though the variability in SSC can significantly influence river habitats and floodplain development [11], and our knowledge about how human activities affect spatiotemporal SSC

 doi:10.20944/preprints202405.1032.v1

patterns in rivers is still rather limited [12–14]. It is evident that understanding sediment dynamics in rivers is crucial, but a major challenge is the lack of field information on SSC. Only a small percentage of the largest rivers on Earth have SSC monitoring sites, making it difficult to gather long-term SSC records and obtain spatial SSC coverage. While in-situ sensors can give insights into high-frequency dynamics, studying SSC in large rivers requires costly and time-consuming field campaigns with a lot of point measurements and observations. This results in an incomplete description of the spatial view of the process in the entire study region.

Satellites can provide a solution to the lack of data for developing long-term, spatially distributed SSC observations. Compared to local SSC gauging stations, satellite images can cover larger geographical areas with relatively high revisit time (i.e., temporal resolution) and detail (i.e., spatial resolution) for prolonged periods. This results in faster processing and reduced costs when compared with field campaigns. Recent studies have demonstrated the reliability of using satellite-derived information to investigate fluvial morphology and SSC in selected river reaches [15–19].

Previous research has primarily focused on large rivers, estuaries [20,21], lakes [22,23], reservoirs [24,25] and coastal [26,27] and marine areas, using remote sensing data with a spatial resolution of 500-1000 m [28–30]. However, more accurate information might be needed in the case of rivers characterized by large spatiotemporal variability in SSC, such as the Changjiang River, and therefore more high-resolute satellite images should be exploited. Therefore, the current work takes advantage of Sentinel-2 images. With respect to the medium-resolution images used so far (i.e., MODIS, MERIS and OLCI), data with the higher spatial resolution coming from the more recent Sentinel-2 Mission of the Copernicus European Earth Observation programme (10, 20 and 60 m spatial resolution) have opened new possibilities to investigate small targets [31].

In the Changjiang River Basin, most previous studies have focused on estuaries [32–36] and some large lakes [37–39], while there is still a lack of investigations on the main channel, mostly because of the lack of detailed field information and the challenges posed by retrieving SSC patterns in fast-changing conditions. The current study aims to contribute to this topic, providing a calibrated model that relates local SSC data with water reflectance, to eventually create SSC maps over the Zhijiang-Chenglingji reach in the middle Changjiang River mainstream, analyzing how SSC changed over the period 2017-2022 in correspondence to selected extreme events.

2. Materials and Methods

2.1. Study Area

The Changjiang River is one of the world's largest rivers and has undergone a significant reduction in sediment load in recent decades, due to the effects of dam construction and soil conservation practices [40]. It ranks as the third longest river by length (~6,400 km), the fifth largest in terms of river discharge (~900 km^3/y), and the fourth largest in terms of sediment load (~480 Mt/y) in the world [41]. It has a drainage area of approximately 1.9×10^6 km^2, accounting for nearly 20% of the territory of China. The Changjiang River originates from the Qinghai-Tibet Plateau and stretches west-eastward from central China to the East China Sea. It is usually divided into three sub-basins with the demarcations at the Yichang and Hukou hydraulic stations, i.e., the upper, middle, and lower reaches, primarily based on its spatially varying landscape and climate patterns (Figure 1). The upper, middle, and lower reaches of the Changjiang River are about 4500, 955, and 938 km long, respectively. In this study, we considered the reach from Zhijiang to Chenglingji (~290 km), which belongs to the middle reach of the Changjiang River.

Preprints.org (www.preprints.org) | NOT PEER-REVIEWED | Posted: 15 May 2024 doi:10.20944/preprints202405.1032.v1

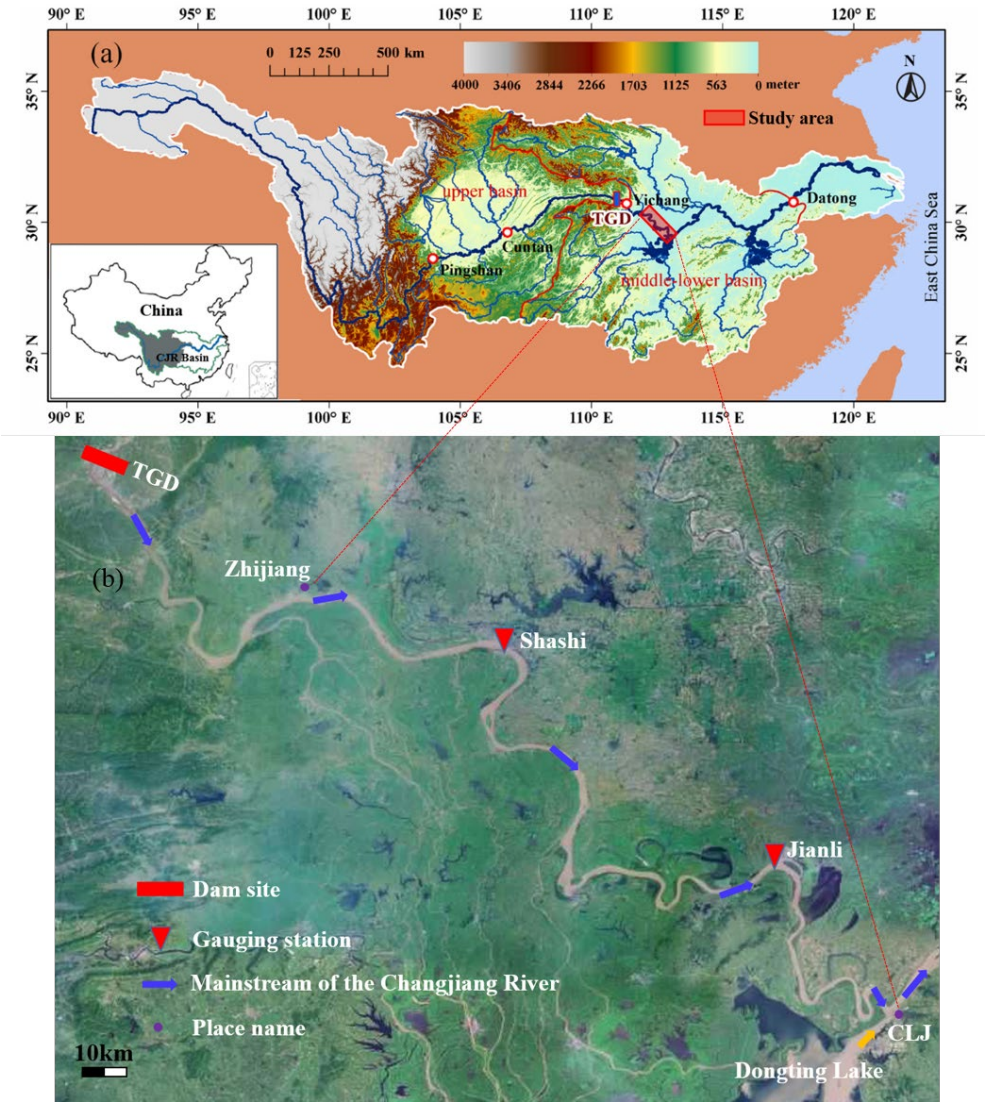

Figure 1. Overview of (a) the Changjiang River Basin, and (b) the study area. TGD=Three Gorges Reservoir; CLJ=Chenglingji.

2.2. Field Data

Table 1 reports water levels, flow discharge and suspended sediment concentration at the two gauging stations of Shashi (SS) and Jianli (JL), measured on the same dates when cloudless Sentinel-2 images were available for the investigated reach. The data were obtained from the Changjiang Water Resources Commission (CWRC) (www.cjw.gov.cn/zwzc/bmgb/), and their consistency was verified.

Table 1. Measured water flow and SSC over the period 2017-2022 at the SS and JL gauging stations.

Date	SS water level [m]	SS discharge [m³/s]	SS sediment concentration [kg/m³]	JL water level [m]	JL discharge [m³/s]	JL sediment concentration [kg/m³]
2017-02-27	31.17	7760	0.036	25.36	7160	0.048
2017-04-28	34.52	13400	0.040	28.68	13400	0.082
2017-06-07	35.82	16200	0.037	29.84	14200	0.060
2017-06-27	37.75	19300	0.063	32.74	17000	0.033

 doi:10.20944/preprints202405.1032.v1

2017-07-17	39.66	23600	0.072	34.34	22200	0.082
2017-08-06	35.23	13500	0.029	30.07	13900	0.056
2017-09-15	36.23	16700	0.047	30.12	15700	0.109
2017-10-30	36.48	17200	0.023	30.51	16800	0.101
2017-11-09	33.23	10100	0.017	28.01	11000	0.057
2017-12-09	31.26	7610	0.016	25.58	8100	0.072
2018-01-08	31.11	7820	0.012	25.13	7510	0.071
2018-02-12	31.11	7670	0.017	25.49	8060	0.083
2018-03-09	31.27	8140	0.012	25.36	7980	0.085
2018-04-03	31.26	8120	0.015	25.72	7600	0.050
2018-04-18	32.42	10200	0.024	26.47	9780	0.132
2018-07-22	39.95	26600	0.850	33.96	24800	1.040
2018-08-16	39.12	25100	0.143	32.35	24000	0.162
2018-10-05	35.01	14700	0.020	29.06	14300	0.120
2018-10-10	36.58	18500	0.025	29.71	17900	0.125
2018-11-29	30.78	7200	0.010	26.06	7490	0.036
2019-01-23	31.57	8580	0.011	26.57	8260	0.052
2019-03-14	30.77	6840	0.018	26.86	6920	0.021
2019-04-08	32.58	10400	0.015	27.50	9880	0.073
2019-05-08	33.40	11400	0.020	28.65	11200	0.053
2019-05-23	37.50	20400	0.037	31.87	18000	0.112
2019-08-01	40.51	28600	0.139	34.30	25800	0.225
2019-08-11	39.79	26700	0.168	33.58	24000	0.244
2019-08-16	37.75	19700	0.091	32.50	19300	0.197
2019-09-30	34.18	13000	0.026	28.44	13800	0.137
2019-11-04	34.59	14900	0.026	28.09	14200	0.126
2019-11-09	33.19	11500	0.022	27.34	12100	0.109
2019-12-04	30.35	7170	0.015	24.78	7310	0.060
2020-02-17	30.25	6770	0.010	25.63	7080	0.024
2020-02-22	30.12	6610	0.012	25.47	6900	0.034
2020-03-18	32.18	9740	0.011	27.18	9750	0.042
2020-04-12	32.61	10200	0.019	28.04	10200	0.036
2020-05-02	31.78	8860	0.018	26.76	9470	0.068
2020-06-01	33.57	12300	0.020	28.28	11800	0.064
2020-08-15	42.12	35400	0.114	35.66	32400	0.167
2020-08-30	41.23	30300	0.653	35.57	27200	0.779
2020-10-29	34.94	14400	0.011	30.28	13500	0.074
2020-11-08	34.09	12900	0.009	28.84	13000	0.092
2021-01-02	31.32	8260	0.012	25.79	9320	0.164
2021-01-12	32.44	10400	0.013	26.66	10700	0.157
2021-02-21	30.27	7230	0.015	24.90	7420	0.051
2021-06-06	34.75	12600	0.017	31.56	12500	0.027
2021-07-26	38.48	21900	0.113	33.01	21200	0.224

 doi:10.20944/preprints202405.1032.v1

2021-07-31	37.13	18300	0.059	32.07	17900	0.141
2021-08-30	39.64	26400	0.079	33.53	25200	0.126
2021-09-14	39.88	27900	0.072	33.68	26100	0.123
2021-09-24	38.24	21600	0.035	32.72	20100	0.100
2021-10-04	37.71	20600	0.036	32.08	19300	0.086
2021-11-08	32.87	11000	0.012	27.70	11000	0.074
2021-11-13	33.04	11300	0.012	27.60	11500	0.084
2022-03-08	31.25	8670	0.010	26.56	8780	0.053
2022-03-28	31.21	8720	0.019	26.28	8760	0.055
2022-04-07	31.39	9030	0.008	26.59	8900	0.042
2022-08-05	34.45	14800	0.016	28.50	14000	0.109
2022-09-04	31.13	9030	0.010	25.54	8970	0.049
2022-09-14	30.60	8260	0.008	25.10	8250	0.053
2022-09-29	29.68	6960	0.012	24.30	7170	0.038
2022-10-14	30.26	7400	0.011	25.38	8030	0.055
2022-10-19	29.76	7060	0.010	24.44	7240	0.061
2022-11-03	29.72	7080	0.010	24.16	7190	0.051
2022-12-08	29.59	6950	0.009	24.08	7040	0.061
2022-12-18	29.54	6920	0.009	23.99	6980	0.041

It is worth noticing that water and sediments are continuously monitored in the two stations, as Figure 2 depicts.

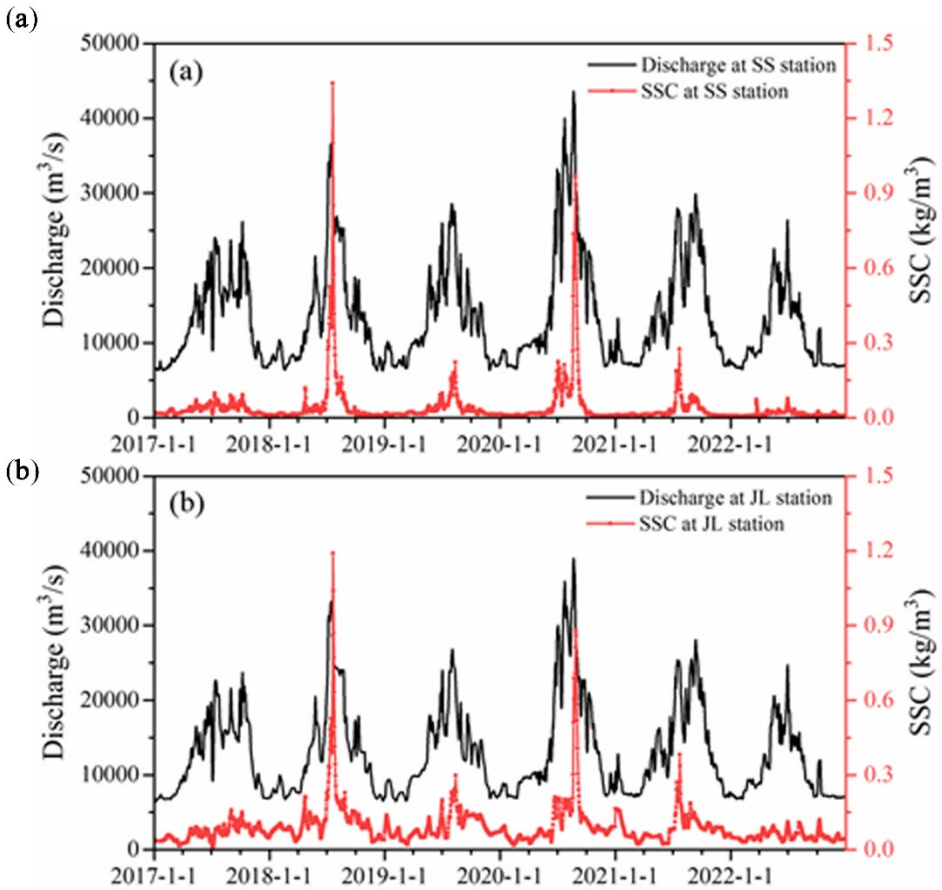

 doi:10.20944/preprints202405.1032.v1

Figure 2. Water discharge and SSC measured at the (**a**) SS and (**b**) JL stations.

2.3. Sentinel-2 dataset

Sentinel-2 data were used in the current study. The Copernicus Sentinel-2 mission consists of two polar-orbiting satellites positioned in a synchronized sun-synchronous orbit, with a 180° phase difference between them. The objective of this mission is to observe changes in land surface conditions. With its broad swath width of 290 kilometres and frequent revisits (10 days at the equator with one satellite, and 5 days with two satellites in cloud-free conditions, resulting in 2-3 days at mid-latitudes), it facilitates the monitoring of alterations on the Earth's surface [42].

Images, downloaded from the Copernicus database directly in the open software QGIS using the plugin Semi-automatic Classification Plugin SCP version 8.2.2 [43], belong to both Level L1C and Level L2A, being the latter atmospherically corrected and the first georeferenced. Images covering the period 2017-2023 with a cloud cover lower than 5% were selected to match the available SSC data. Images were then converted to TOA (Top of Atmosphere) reflectance. This accounts for both the reflectance of the Earth's surface and the influence of the atmosphere on the received light. This conversion normalizes the data for variations in solar irradiance (the amount of sunlight), making it easier to compare and analyze the information captured by the satellite across different conditions

The two satellites Sentinel-2A and Sentinel-2B are equipped with Multi-Spectral Instrument (MSI). This instrument captures data across various spectral bands (Table 2), including four bands at 10 meters resolution in the visible spectrum, covering the wavelengths of blue (490 nm), green (560 nm), red (665 nm), and near-infrared (842 nm). Furthermore, there are six bands at 20 meters resolution, four of which are narrow bands in the vegetation red edge spectral range (705, 740, 775, and 865 nm), along with two longer bands in the shortwave infrared (SWIR) region (1610 and 2190 nm). Additionally, there are three bands at 60-meter resolution dedicated to tasks like atmospheric correction (443 nm for aerosols and 940 nm for water vapour) and cirrus cloud detection (1380 nm) [44].

Table 2. Sentinel-2 band characteristics.

Band	Band Description	Resolution [m]	Central Wavelength [nm]	Bandwidth [nm]
Band 1	Deep blue	60	443	20
Band 2	Blue	10	490	65
Band 3	Green	10	560	35
Band 4	Red	10	665	30
Band 5	Vegetation Red-edge	20	705	15
Band 6	Vegetation Red-edge	20	740	15
Band 7	Vegetation Red-edge	20	783	20
Band 8	Near Infrared	20	842	115
Band 8A	Narrow Near Infrared	20	865	20
Band 9	Water vapour	60	945	20
Band 10	Shortwave infrared - Cirrus	60	1375	30
Band 11	Shortwave infrared 1	20	1610	90
Band 12	Shortwave infrared 2	20	2190	180

To provide a comprehensive evaluation, three Sentinel-2 granules were selected given the large extent of the study area. These granules are also called tiles, which are the minimum indivisible partitions in the MSI sensor reference frame of a given number of lines along the track and detector-

 doi:10.20944/preprints202405.1032.v1

separated [45]. Specifically, the tile IDs are 49REP, 49RFP, and 49RFN, which extensively covered the study area from west to east.

2.4. Reflectance Models

Multiple models able to relate field data and image reflectance exist and were tested in the current application (Table 3) by comparing SSC field and satellite-retrieved information. For a full description of the models readers can refer to the cited literature.

Table 3. Tested models to relate SSC and turbidity to image reflectance.

Model	Reference
R705 - R740	Härmä et al., 2001 [46]
R783 / R490	Yuan et al., 2019 [47]
R665	Caballero et al., 2018 [48]
(R560+R705) / (R560+R665)	Hou et al., 2017 [49]
R665 / R560	Hou et al., 2017 [49]
R705	Kallio et al., 2001 [50]
R490 / (R443+R560)	Lathrop & Lillesand,1989 [51]
R783	Zhan et al., 2022 [27]
(R560-R490) / (R560+R490)	Erena et al., 2019 [52]
R783 * R705/R490	Zhan et al., 2022 [27]
R705 * R705/R490	Zhan et al., 2022 [27]
(R783/R490) + (R665/R560)	Zhan et al., 2022 [27]
(R443-R665) / (R560 –R665)	Härmä et al., 2001 [46]
R705 / (R560+R665)	Koponen et al., 2007 [53]
R842 / (R560+R665+R1610)	Duan et al., 2024 [18]
R490	Petus et al., 2010 [54]

3. Results

3.1. Satellite Image Calibration

To retrieve a relationship between measured SSC and band reflectance, images should be first pre-processed to account for atmospheric correction, and then the reflectance values could be derived. To correlate measured SSC and reflectance, 9 pixels neighbouring each station were analysed in QGIS, and the reflectance value was then averaged to reduce local errors. Values were then tabulated and different relationships for each model (see Table 3) were tested, to select the best-fitting model for both stations (i.e., higher R^2).

As visible in Table 4, all models present an R^2 lower than 0.5, with the ratio R665/R560 (band 4/band 3) being the best model.

Table 4. Performance of tested SSC-reflectance model.

Model	R^2
R705 - R740	0.05
R783 / R490	0.13
R665	0.27
(R560+R705) / (R560+R665)	0.04

 doi:10.20944/preprints202405.1032.v1

R665 / R560	0.43
R705	0.20
R490 / (R443+R560)	0.07
R783	0.32
(R560-R490) / (R560+R490)	0.01
R783 * R705/R490	0.22
R705 * R705/R490	0.35
(R783/R490) + (R665/R560)	0.33
(R443-R665) / (R560 –R665)	0.28
R705 / (R560+R665)	0.37
R842 / (R560+R665+R1610)	0.12
R490	0.25

The model R665/R560 performs better than the other, and it was therefore selected for further application using eq. (1):

$$SSC = 0.2139\frac{R665}{R560} - 0.1033 \quad (1)$$

3.2. Application to Extreme Events

The algorithm was applied considering six different conditions, characterized by high water discharge and/or high SSC measured at the gauging stations (Table 5). As visible, events having a significant water discharge might mobilize a relatively low amount of sediments, as happened on August 30, 2021.

Table 5. Details of conditions. ++/-- indicates a value significantly higher/lower than the average, while +/- indicates values just above/below the average. Absolute values are reported in Table 1.

Date	Q	SSC
2017-07-17	+	+
2018-01-08	--	--
2018-07-22	++	++
2019-08-16	+	+
2020-08-30	++	++
2021-08-30	++	+

From Figure 3, it is evident that high flow conditions generally transport significant suspended sediment along the whole reach, covering both the main channel and the secondary ones. Similarly, low flow conditions are unable to transport a significant amount of material, therefore resulting in lower concentration transported only in the middle of the channel.

It is worth noticing here that, in July 2017, SSC increased in the lower part of the study area, starting from about 10 km upstream of JL. This might be due to significant riverbank erosion in this area. Such instability is mainly caused by a decrease in SSC during normal flow conditions due to the cascade reservoirs present upstream of the study reach [55], which represents a current worrying risk to flood protection in the area [56]. In fact, according to the statistics provided by the Changjiang Water Resource Committee in 2021, a total of 1046 riverbank collapses occurred, with a cumulative length of approximately 760 km in the middle-lower reaches of the Changjiang River from 2003 to 2021 [57].

 doi:10.20944/preprints202405.1032.v1

Looking at the other events analysed in the current study, no significant spatial differences are visible, meaning that no localized sources of sediment impacted the study area during such extreme events.

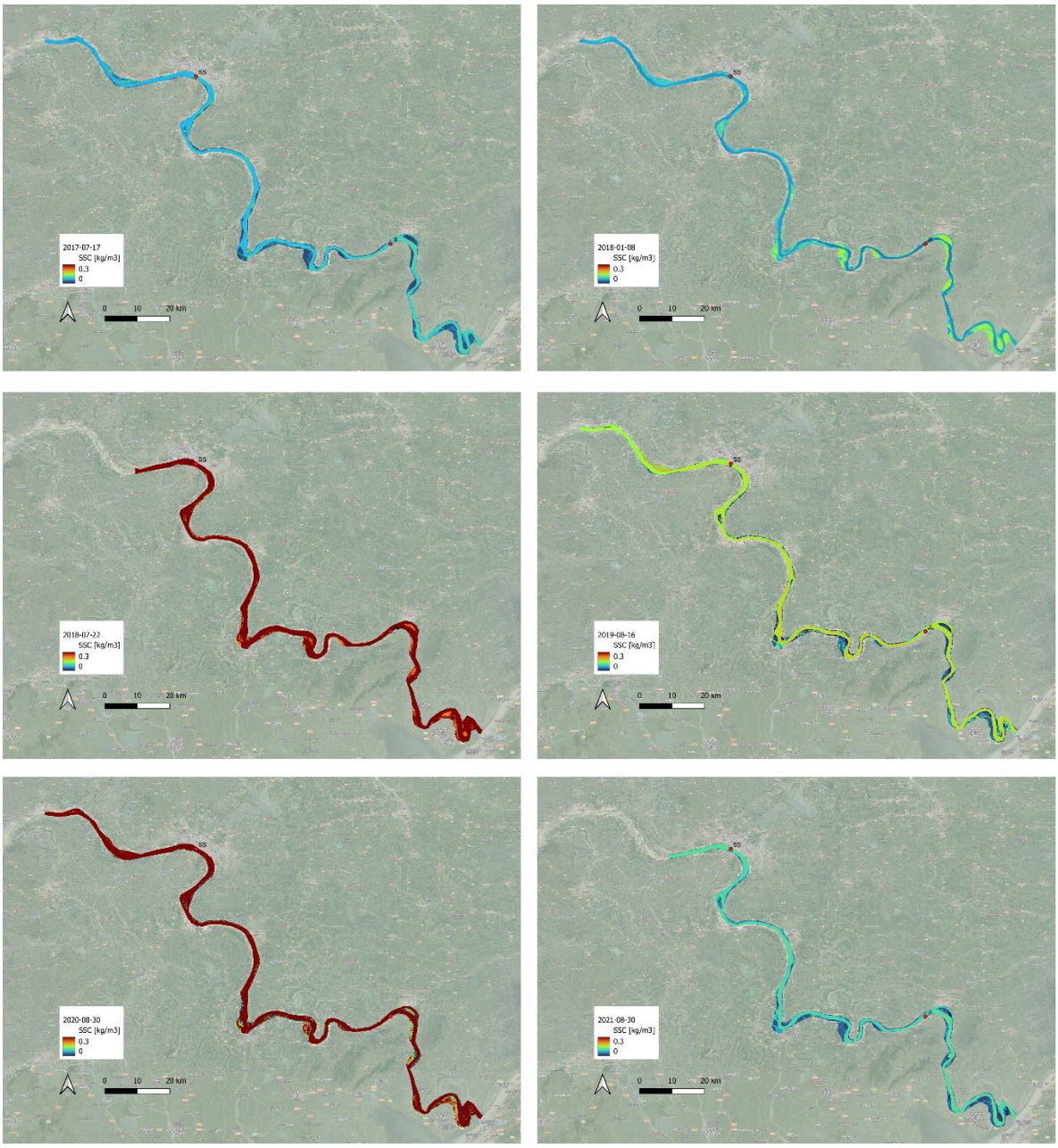

Figure 3. SSC simulated on different dates (see Table 5).

4. Discussion

4.1. Uncertainties in SSC Retrieval from Remote Sensing

It has been found that only about 10% of the signals that were received by the satellite sensors are from water bodies. The rest of the signals are mainly originating from atmospheric scattering, topographic and soil brightness effects, as mentioned in studies conducted by Huete et al. [58]), Borgogno-Mondino et al. [59], Boothroyd et al. [60], and Duan et al. [18]. Thus, it is crucial to perform atmospheric correction to derive accurate colour-related water parameters [61]. As rivers generally exhibit high turbidity and complex optical characteristics, the assumption of zero water-leaving radiance in the near-infrared band [62] might be no longer valid in such environments. Previous

 doi:10.20944/preprints202405.1032.v1

research has shown that correcting for atmospheric effects using the short-wave infrared band can help deal with the issue of water-leaving signals in satellite imagery. However, in the case of very turbid waters, like those in the Changjiang River during floods, there is still a noticeable water-leaving signal in the short-wave infrared band [17].

In addition to the challenges posed by turbid waters, the effects of land adjacency may significantly impact the signal in the short-wave infrared band, even in cases where the water-leaving radiance is negligible [61], especially in narrow rivers crossing urban centres [17]. Additionally, the reflection of direct sunlight at the air-water interface, known as sunglint, may also have an impact on the retrieval of water-leaving radiance [63]. The combination of all these challenges often leads to uncertainties in estimating remote sensing reflectance after atmospheric correction, further affecting the results of SSC retrieval [18].

Besides uncertainties connected to atmospheric correction, also differences in sediment particle size may contribute to the uncertainties in SSC retrieval. As past investigations have shown [34,64], particle size and distribution could impact surface reflectance altering the backscattering coefficient, with differences increased with increasing wavelength. SSC particle size was highly dynamic in this area as a result of river scouring and the replenishment of fine sediment [65]. In addition, as the erosion has lasted for over 20 years, the replenished and restored fine riverbed particles as suspended sediment showed an overall decreasing trend. To further corroborate the results presented in the current study, future studies should consider the distribution of sediment particle sizes and their influence on remote sensing models.

It is also worth noticing that, with respect to more still water present in small/medium lakes and reservoirs, a large range of hydrological conditions should be considered in estimating SSC in rivers, as water optical properties might have significant variations in the dry and wet seasons [17]. Therefore, selected calibration and validation data should be sufficient and cover as many different seasons as possible. At the same time, the need for covering a broader spectrum of hydrological conditions SCC values might result in less accurate models, as suggested by the current research, especially in watercourses affected by significant variations of SSC due to climate variations and human intervention.

SSC models derived by using band ratio, as made in the current work (eq. (1)) could implicitly compensate for some uncertainty in remote sensing reflectance estimation [49]. Thus, since the spectral variation in the backscattering coefficient of suspended sediments is smooth, band ratios can mitigate the impact of differences in sediment particle size [66]. To further mitigate the uncertainty in reflectance retrieval, values were derived from multiple pixels located around the gauging stations, eventually deriving a spatial average.

4.2. Driving Forces of SSC Transport

SSC in rivers is usually positively correlated with water discharge, as also demonstrated by past investigations focused on the middle reach of the Changjiang River [67,68] and the Yellow River [18] in China, or on the Indian Chandra River [69] and the River Rhine and the Celone River in Europe [70].

However, anthropogenic alterations such as the presence of reservoirs could alter this trend, reducing the correlation between water discharge and SSC, therefore complicating the estimation of SSC as a function of water discharge via classical sediment rating curves [71]. For example, Zhang et al. [23] reported that, after the construction of the Xiaolangdi reservoir on the Yellow River, the correlation between water flow and SSC decreased at several hydrological stations, as the reservoir has a minor impact on annual water flow, but a significant impact on sediment transport in the lower reach, leading to a substantial decrease in SSC. For a river system undergoing significant sediment load decline, river channel self-adjustment is an important factor driving the recruitment of SSC from bed and bank erosion. It was reported that from the impoundment of TGR in 2003 to 2021, the whole middle reach of the Changjiang River was scouring, resulting in a gradual SSC recovery from the dam site downstream to Chenglingji [72].

 doi:10.20944/preprints202405.1032.v1

5. Conclusions

In the current work, remote sensing was combined with field data to investigate SSC dynamics along the Zhijiang-Yueyang reach of the Changjiang River, and how the quantity of transported sediment changed in response to extreme high and low flow conditions, considering six selected events during the period 2017-2022.

Despite uncertainties in calibration, this application has shown the potential of using satellite images and band reflectance to map spatiotemporal changes of SSC, eventually overcoming limitations due to the very local nature of using field sampling. Multiple models combining band reflectance were tested to derive the most suitable one for describing the observed SSC variability, highlighting the strengths and weaknesses of the proposed approach. Indeed, monitoring from above highly variable conditions of SSC, which are typical of riverine environments, might be very challenging, and a large volume of information is needed to derive good-fitting relationships. To address this point, future investigations will consider a longer reach and extended temporal horizons, eventually combining satellite data at different spatiotemporal resolutions.

Author Contributions: Conceptualization, M.N. and C.G.; methodology, M.N.; calibration and validation, M.N.; formal analysis, M.N. and C.G.; data curation, M.N. and C.G.; writing—original draft preparation, M.N. and C.G.; writing—review and editing, M.N., C.G.; visualization, M.N. and C.G. All authors have read and agreed to the published version of the manuscript.

Data Availability Statement: The used data are provided in the article.

Acknowledgements: The work of M.N. was supported by a subsidy from the Polish Ministry of Education and Science for the Institute of Geophysics, Polish Academy of Sciences.

Conflicts of Interest: The authors declare no conflicts of interest.

References

1. Leopold, L.; Wolman, M.; Miller, J. *Fluvial Processes in Geomorphology* **1964**. San Francisco, USA.
2. Nones, M. Remote sensing and GIS techniques to monitor morphological changes along the middle-lower Vistula river, Poland. *International Journal of River Basin Management* **2021**, 19(3), 345-357.
3. Hamidifar, H.; Nones, M.; Rowinski, P.M. Flood modeling and fluvial dynamics: A scoping review on the role of sediment transport. *Earth-Science Reviews* **2024**, 253, 104775.
4. Bernhardt, E.S.; Savoy, P.; Vlah, M.J.; Appling, A.P.; Koenig, L.E.; ...; Grimm, N.B. Light and flow regimes regulate the metabolism of rivers. *Proc. National Academy of Sciences* **2022**, 119(8), e2121976119.
5. Walling, D.E.; Russell, M.A.; Webb, B.W. Controls on the nutrient content of suspended sediment transported by British rivers. *Science of the Total Environment* **2001**, 266(1-3), 113-123.
6. Syvitski, J.P.; Vörösmarty, C.J.; Kettner, A.; Green, P. Impact of humans on the flux of terrestrial sediment to the global coastal ocean. *Science* **2005**, 308(5720), 376-380.
7. Wotton, R.S. Do benthic biologists pay enough attention to aggregates formed in the water column of streams and rivers? *Journal of the North American Benthological Society* **2007**, 26(1), 1-11.
8. Ho, Q.N.; Fettweis, M.; Spencer, K.L.; Lee, B.J., Flocculation with heterogeneous composition in water environments: A review. *Water Research* **2022**, 118147.
9. Waldschläger, K.; Brückner, M.Z.; Almroth, B.C.; Hackney, C.R.; Adyel, T.M.; Alimi, O.S., ...; Wu, N. Learning from natural sediments to tackle microplastics challenges: A multidisciplinary perspective. *Earth-Science Reviews* **2022**, 228, 104021.
10. Mohsen, A.; Kovács, F.; Kiss, T. Riverine Microplastic Quantification: A Novel Approach Integrating Satellite Images, Neural Network, and Suspended Sediment Data as a Proxy. *Sensors* **2023**, 23(23), 9505.
11. Wohl, E.; Bledsoe, B.P.; Jacobson, R.B.; Poff, N.L.; Rathburn, S.L.; Walters, D.M.; Wilcox, A.C. The natural sediment regime in rivers: Broadening the foundation for ecosystem management. *BioScience* **2015**, 65(4), 358-371.
12. Aleixo, R.; Guerrero, M.; Nones, M.; Ruther, N. Applying ADCPs for long-term monitoring of SSC in rivers. *Water Resources Research* **2020**, 56(1), e2019WR026087.
13. Dethier, E.N.; Renshaw, C.E.; Magilligan, F.J. Rapid changes to global river suspended sediment flux by humans. *Science*, **2022**. 376(6600), 1447-1452.
14. Gardner, J.; Pavelsky, T.; Topp, S.; Yang, X.; Ross, M.R.; Cohen, S. Human activities change suspended sediment concentration along rivers. *Environmental Research Letters* **2023**, 18(6), 064032.
15. Curran, P.J.; Novo, E.M.M. The relationship between suspended sediment concentration and remotely sensed spectral radiance: A review. *Journal of Coastal Research* **1988**, 351-368.

16. Umar, M.; Rhoads, B.L.; Greenberg, J.A. Use of multispectral satellite remote sensing to assess mixing of suspended sediment downstream of large river confluences. *Journal of Hydrology* **2018**, 556, 325-338.
17. Zhang, C.; Liu, Y.; Chen, X.; Gao, Y. Estimation of suspended sediment concentration in the Yangtze main stream based on sentinel-2 MSI data. *Remote Sensing* **2022**, 14(18), 4446.
18. Duan, M.; Qiu, Z.; Li, R.; Li, K.; Yu, S.; Liu, D. Monitoring Suspended Sediment Transport in the Lower Yellow River using Landsat Observations. *Remote Sensing* **2024**, 16(2), 229.
19. Nones, M.; Guerrero, M.; Schippa, L.; Cavalieri, I. Remote sensing assessment of anthropogenic and climate variation effects on river channel morphology and vegetation: The Po River case in Italy. *Earth Surface Processes and Landforms* **2024**, 49(5), 1632-1652.
20. Zhang, M.; Ma, R.; Li, J.; Zhang, B.; Duan, H. A Validation Study of an Improved SWIR Iterative Atmospheric Correction Algorithm for MODIS-Aqua Measurements in Lake Taihu, China. *IEEE Trans. Geosci. Remote Sens.* **2014**, 52, 4686-4695.
21. Zhan, W.; Wu, J.; Wei, X.; Tang, S.; Zhan, H. Spatio-temporal variation of the suspended sediment concentration in the Pearl River Estuary observed by MODIS during 2003–2015. *Continental Shelf Research* **2019**, 172, 22-32.
22. Jally, S.K.; Mishra, A.K.; Balabantaray, S. Retrieval of suspended sediment concentration of the Chilika Lake, India using Landsat-8 OLI satellite data. *Environ. Earth Sci.* **2021**, 80, 298.
23. Zhang, M.; Dong, Q.; Cui, T.; Xue, C.; Zhang, S. Suspended sediment monitoring and assessment for Yellow River estuary from Landsat TM and ETM+ imagery. *Remote Sens. Environ.* **2014**, 146, 136–147.
24. Robert, E.; Grippa, M.; Kergoat, L.; Pinet, S.; Gal, L.; Cochonneau, G.; Martinez, J.-M. Monitoring water turbidity and surface suspended sediment concentration of the Bagre Reservoir (Burkina Faso) using MODIS and field reflectance data. Int. *J. Appl. Earth Obs. Geoinf.* **2016**, 52, 243–251.
25. Zhang, Y.; Zhang, Y.; Shi, K.; Zha, Y.; Zhou, Y.; Liu, M.A. Landsat 8 OLI-based, semianalytical model for estimating the total suspended matter concentration in the slightly turbid Xin'anjiang Reservoir (China). *IEEE J. Sel. Top. Appl. Earth Obs. Remote Sens*. **2016**, 9, 398–413.
26. Pitchaikani, J.S.; Ramakrishnan, R.; Bhaskaran, P.K.; Ilangovan, D.; Rajawat, A.S. Development of regional algorithm to estimate suspended sediment concentration (SSC) based on the remotely sensed reflectance and field observations for the Hooghly estuary and West Bengal coastal waters. *Journal of the Indian Society of Remote Sensing* **2019**, 47, 177-183.
27. Zhan, Y.; Delegido, J.; Erena, M.; Soria, J.M.; Ruiz-Verdú, A.; Urrego, P.; ...; Moreno, J. Mar Menor lagoon (SE Spain) chlorophyll-a and turbidity estimation with Sentinel-2. *Limnetica* **2022**, 41(2), 305-323.
28. Luo, X.; Wang, J.; Chen, G.; Zhu, S.; Huo, Z.; Liu, X.; Deng, W. Research on Distribution of Suspended Sediment Concentration in Long Time Series Based on Mid-Resolution Imaging Spectrometer Data and Quantile Trend Analysis. *Reg. Stud. Mar. Sci.* **2020**, 39, 101399.
29. Wang, W.; Jiang, W. Study on the Seasonal Variation of the Suspended Sediment Distribution and Transportation in the East China Seas Based on SeaWiFS Data. *J. Ocean Univ. China* **2008**, 7, 385–392.
30. Womber, Z.R.; Zimale, F.A.; Kebedew, M.G.; Asers, B.W.; DeLuca, N.M.; Guzman, C.D.; Tilahun, S.A.; Zaitchik, B.F. Estimation of Suspended Sediment Concentration from Remote Sensing and In Situ Measurement over Lake Tana, Ethiopia. *Adv. Civ. Eng.* **2021**, 9948780.
31. Filippucci, P.; Brocca, L.; Bonafoni, S.; Saltalippi, C.; Wagner, W.; Tarpanelli, A. Sentinel-2 high-resolution data for river discharge monitoring. *Remote Sensing of Environment* **2022**, 281, 113255.
32. Chen, J.; D'Sa, E.; Cui, T.; Zhang, X. A semi-analytical total suspended sediment retrieval model in turbid coastal waters: A case study in Changjiang River Estuary. *Opt. Express* **2013**, 21, 13018–13031.
33. Han, Z.; Jin, Y.Q.; Yun, C.X. Suspended sediment concentrations in the Yangtze River estuary retrieved from the CMODIS data. *Int. J. Remote Sens.* **2006**, 27, 4329–4336.
34. Shen, F.; Verhoef, W.; Zhou, Y.; Salama, M.; Liu, X. Satellite estimates of wide-range suspended sediment concentrations in Changjiang (Yangtze) estuary using MERIS data. *Estuaries Coasts* **2010**, 33, 1420–1429.
35. Sokoletsky, L.; Yang, X.; Shen, F. MODIS-based retrieval of suspended sediment concentration and diffuse attenuation coefficient in Chinese estuarine and coastal waters. In *Ocean Remote Sensing and Monitoring from Space*; SPIE: Beijing, China, **2014**; p. 926119.
36. Wang, C.; Li, D.; Wang, D.; Chen, S.; Liu, W. A total suspended sediment retrieval model for multiple estuaries and coasts by Landsat imageries. In *Proceedings of the 2016 4th International Workshop on Earth Observation and Remote Sensing Applications (EORSA)*, Guangzhou, China, 4–6 July 2016; IEEE: Piscataway, NJ, USA, **2016**; pp. 150–152.
37. Ma, R.; Dai, J. Investigation of chlorophyll-a and total suspended matter concentrations using Landsat ETM and field spectral measurement in Taihu Lake, China. *Int. J. Remote Sens.* **2005**, 26, 2779–2795.
38. Wu, G.; Cui, L.; He, J.; Duan, H.; Fei, T.; Liu, Y. Comparison of MODIS-based models for retrieving suspended particulate matter concentrations in Poyang Lake, China. *Int. J. Appl. Earth Obs. Geoinf.* **2013**, 24, 63–72.

 doi:10.20944/preprints202405.1032.v1

39. Zheng, Z.; Li, Y.; Guo, Y.; Xu, Y.; Liu, G.; Du, C. Landsat-based long-term monitoring of total suspended matter concentration pattern change in the wet season for Dongting Lake, China. *Remote Sensing* **2015**, 7, 13975–13999.
40. Best, J. Anthropogenic stresses on the world's big rivers. *Nature Geoscience* **2019**, 12 (1), 7-21.
41. Milliman, J.D.; Farnsworth, K.L. River discharge to the coastal ocean: A global synthesis. Cambridge University Press 2013, 382 Pages.
42. Spoto, F.; Sy, O.; Laberinti, P.; Martimort, P.; Fernandez, V.; Colin, O.; Hoersch, B.; Meygret, A. Overview of Sentinel-2. *IEEE International Geoscience and Remote Sensing Symposium*, Munich, Germany, **2012**, 1707-1710.
43. Congedo, L. Semi-Automatic Classification Plugin: A Python tool for the download and processing of remote sensing images in QGIS. *Journal of Open Source Software* **2021**, 6(64), 3172.
44. Segarra, J.; Buchaillot, M.L.; Araus, J.L.; Kefauver, S.C. Remote sensing for precision agriculture: Sentinel-2 improved features and applications. *Agronomy* **2020**, 10(5), 641.
45. Gao, X.; Chi, H.; Huang, J.; Han, Y.; Li, Y.; Ling, F. Comparison of Cloud-Mask Algorithms and Machine-Learning Methods Using Sentinel-2 Imagery for Mapping Paddy Rice in Jianghan Plain. *Remote Sensing* **2024**, 16,7, 1305.
46. Härmä, P.; Vepsalainen, J.; Hannonen, T.; Pyhalahti, T.; Kamari, J.; Kallio, K.; ...; Koponen, S. Detection of water quality using simulated satellite data and semi-empirical algorithms in Finland. *Science of the Total Environment* **2001**, 268, 107–121.
47. Yuan, L.; Yulong, G.; Chunmei, C.; Yibo, Z.; Yaoduo, H.; Zhong, X.; Shun, B. Remote estimation of total suspended matter concentration in the Hangzhou Bay based on OLCI and its water color product applicability analysis. *Haiyang Xuebao* **2019**, 41(9), 156-169.
48. Caballero, I.; Steinmetz, F.; Navarro, G.. Evaluation of the first year of operational Sentinel-2A data for retrieval of suspended solids in medium-to high-turbidity waters. *Remote Sensing* **2018**, 10(7), 982.
49. Hou, X.; Feng, L.; Chen, X.; Sun, D.; Shi, K. Fifteen-year monitoring of the turbidity dynamics in large lakes and reservoirs in the middle and lower basin of the Yangtze River, China. *Remote Sensing of Environment* **2017**, 190, 107-121.
50. Kallio, K.; Kutser, T.; Hannonen, T.; Koponen, S.; Pulliainen, J.; Vepsalainen, J.; Pyhalahti, T. Retrieval of water quality from airborne imaging spectrometry of various lake types in different seasons. *Science of the Total Environment* **2001**, 268, 59-77.
51. Lathrop, R.G.; Lillesand, T.M. Monitoring water quality and river plume transport in Green Bay, Lake Michigan with SPOT-1 imagery. *Photogrammetric Engineering and Remote Sensing* **1989**, 55, 349–354.
52. Erena, M.; Domínguez, J.A.; Aguado-Giménez, F.; Soria, J.; García-Galiano, S. Monitoring Coastal Lagoon Water Quality through Remote Sensing: The Mar Menor as a Case Study. *Water* **2019**, 11(7), 1468.
53. Koponen, S.; Attila, J.; Pulliainen, J.; Kallio, K.; Pyhälahti, T.; Lindfors, A.; Rasmus, K.; Hallikainen, M. A case study of airborne and satellite remote sensing of a spring bloom event in the Gulf of Finland. *Continental Shelf Research* **2007**, 27(2), 228-244.
54. Petus, C.; Chust, G.; Gohin, F.; Doxaran, D.; Froidefond, J.M.; Sagarminaga, Y. Estimating turbidity and total suspended matter in the Adour River plume (South Bay of Biscay) using MODIS 250-m imagery. *Continental Shelf Research* **2010**, 30(5), 379-392.
55. Wu, X.; Xiang, X.; Chen, X.; Zhang, X.; Hua, W. Effects of cascade reservoir dams on the streamflow and sediment transport in the Wujiang River basin of the Yangtze River, China. *Inland Waters* **2018**, 8(2), 216-228.
56. Nakayama, T.; Shankman, D. Impact of the Three-Gorges Dam and water transfer project on Changjiang floods. *Global and Planetary Change* **2013**, 100, 38-50.
57. Changjiang Water Resource Committee. *Bulletin of the Yangtze River sediment* **2021**. Available at http://www.cjh.com.cn/.
58. Huete, A.; Didan, K.; Miura, T.; Rodriguez, E.P.; Gao, X.; Ferreira, L.G. Overview of the Radiometric and Biophysical Performance of the MODIS Vegetation Indices. *Remote Sensing of Environment* **2002**, 83 (1-2), 195–213.
59. Borgogno-Mondino, E.; Lessio, A.; Gomarasca, M.A. A Fast Operative Method for NDVI Uncertainty Estimation and its Role in Vegetation Analysis. *Eur. J. Remote Sensing* **2016**, 49 (1), 137–156.
60. Boothroyd, R.J.; Nones, M.; Guerrero, M. Deriving planform morphology and vegetation coverage from remote sensing to support river management applications. *Frontiers in Environmental Science* **2021**, 9, 657354.
61. Feng, L.; Hu, C. Land Adjacency Effects on MODIS Aqua Top-of-atmosphere Radiance in the Shortwave Infrared: Statistical Assessment and Correction. *JGR Ocean* **2017**, 122, 4802–4818.
62. Greb, S.; Dekker, A.; Binding, C. *Earth Observations in Support of Global Water Quality Monitoring*. International Ocean Colour Coordinating Group: Dartmouth, NS, Canada, **2018**; ISBN 978-1-896246-67-3.
63. Fell, F. A Contrast Minimization Approach to Remove Sun Glint in Landsat 8 Imagery. *Remote Sensing* **2022**, 14, 4643.

 doi:10.20944/preprints202405.1032.v1

64. Forget, P.; Ouillon, S.; Lahet, F.; Broche, P. Inversion of reflectance spectra of nonchlorophyllous turbid coastal waters. *Remote Sensing of Environment* **1999**, 68(3), 264-272.
65. Yang, Y.; Zheng, J.; Zhu, L.; Zhang, H.; Wang, J.. Influence of the Three Gorges Dam on the transport and sorting of coarse and fine sediments downstream of the dam. *Journal of Hydrology* **2022**, 128654.
66. Doxaran, D.; Froidefond, J.-M.; Lavender, S.; Castaing, P. Spectral Signature of Highly Turbid Waters Application with SPOT Data to Quantify Suspended Particulate Matter Concentrations. *Remote Sens. Environ.* **2002**, 81, 149–161.
67. Yang, S.; Ding, P.; Chen, S. Temporal Change in Bed Level of a River Mouth Channel, Yangtze River Mouth: With Emphasis on the Response to River Discharge and Storm. *J. Coast. Res.* **2001**, 297–308.
68. Dai, Z.; Fagherazzi, S.; Mei, X.; Gao, J. Decline in Suspended Sediment Concentration Delivered by the Changjiang (Yangtze River into the East China Sea between 1956 and 2013. *Geomorphology* **2016**, 268, 123–132.
69. Singh, A.T.; Sharma, P.; Sharma, C.; Laluraj, C.M.; Patel, L.; Pratap, B.; Oulkar, S.; Thamban, M. Water Discharge and Suspended Sediment Dynamics in the Chandra River, Western Himalaya. *J. Earth Syst. Sci.* **2020**, 129, 206.
70. Vercruysse, K.; Grabowski, R.C.; Rickson, R.J., Suspended sediment transport dynamics in rivers: Multi-scale drivers of temporal variation. *Earth-Science Reviews* **2017**, 166, 38-52.
71. Horowitz, A.J. An evaluation of sediment rating curves for estimating suspended sediment concentrations for subsequent flux calculations. *Hydrol. Process.* **2003**, 17, 3387-3409.
72. Sun, J.; Zhang, F.; Zhang, X.; Lin, B., Yang, Z., Yuan, B.; Falconer, R.A. Severely declining suspended sediment concentration in the heavily dammed Changjiang fluvial system. *Water Resources Research* **2021**, 57 (11), e2021WR030370.